Supplementary Information

The novel pathogenesis mediated by multiple RTK signals is uncovered in newly developed retinopathy mouse model

Hideyuki Kitahara[a, b], Sayaka Kajikawa[a], Yoko Ishii[a], Seiji Yamamoto[a, *], Takeru Hamashima[a], Erika Azuma[a, c], Hikari Sato[d], Takako Matsushima[a], Masabumi Shibuya[e], Yutaka Shimada[b], Masakiyo Sasahara[a, *]

[a] *Department of Pathology, Graduate School of Medicine and Pharmaceutical Sciences, University of Toyama, 2630 Sugitani, Toyama-shi, Toyama 930-0194, Japan*

[b] *Department of Japanese Oriental Medicine, Graduate School of Medicine and Pharmaceutical Sciences, University of Toyama, 2630 Sugitani, Toyama-shi, Toyama 930-0194, Japan*

[c] *Department of Technology Development, Toyama Technology Center, Astellas Pharma Tech Co., Ltd., 2-178 Kojin-machi, Toyama-shi, Toyama 930-0809, Japan*

[d] *Department of Neurosurgery, Tokyo General Hospital, 3-15-2 Egota, Nakano-ku, Tokyo 165-0022, Japan*

[e] *Department of Research and Education, Jobu University, 634-1 Toyazuka-machi, Isesaki-shi, Gunma 372-8588, Japan*

[*] Corresponding authors.
Seiji Yamamoto, Ph.D. (seiyama@med.u-toyama.ac.jp, seiyama.flyfishing@gmail.com)
Masakiyo Sasahara, M.D., Ph.D. (sasahara@med.u-toyama.ac.jp)

Supplementary Experimental Procedures

Genotyping and primer sequences

The mouse tail was lysed using SNET buffer (20 mM Tris, 5 mM EDTA, 400 mM NaCl, 0.3% SDS; Nacalai Tesque, Kyoto, Japan) with 10 mg/mL proteinase K (Sigma-Aldrich, St. Louis, MO, USA), and PCR was performed in a C1000 thermal cycler (Bio-Rad Laboratories, Hercules, CA, USA) using Ampdirect Plus (Nacalai Tesque).

Pdgfrb$^{flox/flox}$

Forward: 5′-TTCTTGTCTGAGAGCCTGTTGTGTGATGGA-3′

Reverse: 5′-TGTCTGCAGATCTCTAGCCTTGGGGAAATC-3′

Nestin-Cre

Forward: 5′- GTACTTTCTGTGACTGTCAGCTATCGCTTTGTAAAAC -3′

Reverse: 5′- CAGCACCAGTGTGGAGCTGCACAC -3′

R26R-mCherry

pA1: 5′- AAGGGGGAGGATTGGGAAGACA -3′

phil1: 5′- AAAGTCGCTCTGAGTTGTTAT -3′

phil3: 5′- GGAGCGGGAGAAATGGATATG -3′

Flt1TK$^{-/-}$

17F: 5′- ACCCTCTATACCTGGTCAATTGATGCAAAG -3′

17R: 5′- TGCAAACTCCCACTTGCTGGCATCATAG -3′

PGK-Neo: 5′- GCTAAAGCGCATGCTCCAGACTGCCTTG -3′

Antibodies for immunofluorescence

The following primary antibodies were used: hamster monoclonal anti-CD31 (1:100; Merck Millipore, Billerica, MA, USA), rabbit polyclonal anti-NG2 (1:100; Merck Millipore), rat monoclonal anti-CD13 (1:100; AbD Serotec, Kidlington, UK), rabbit polyclonal anti-collagen type IV (1:500; Merck Millipore), mouse monoclonal anti-αSMA conjugated with FITC or Cy3 (1:500; Sigma-Aldrich), rabbit polyclonal anti-NeuN (1:500; Abcam, Cambridge, MA, USA), rabbit polyclonal anti-Glutamine synthetase (1:500; Abcam), rabbit polyclonal anti-PKCα (1:100; Abcam), rabbit polyclonal anti-Calretinin (1:1,000; Swant, Marly, Switzerland), rabbit monoclonal anti-Calbindin (1:400; Cell Signaling, Danvers, MA, USA), rabbit polyclonal anti-Recoverin (1:50; Novus Biologicals, Littleton, CO, USA), rabbit polyclonal anti-GFAP (1:500; Dako, Glostrup, Denmark), goat polyclonal anti-PDGFRα (1:50; Neuromics, Edina, MN, USA), rat monoclonal anti-PDGFRβ (1:50; eBioscience, San Diego, CA, USA), mouse monoclonal anti-8-OHdG (1:100;

NIKKEN SEIL, Tokyo, Japan), rabbit polyclonal anti-SQSTM1 (1:500; Wako, Osaka, Japan), rabbit polyclonal anti-Collagen type I (1:200; Abcam) and rabbit polyclonal anti-CTGF (1:200; Abcam). Positive immunoreactions were visualized using the following fluorescent dye-conjugated secondary antibodies at 4°C overnight: Alexa-Fluor488-, Alexa-Fluor568-, or Alexa-Fluor633-conjugated secondary antibodies (Life Technologies Corporation, Carlsbad, CA, USA) and Alexa-Fluor488-, Cy3-, or Alexa-Fluor647-conjugated secondary antibodies (Jackson ImmunoResearch Inc., West Grove, PA, USA) were used at 1:500 dilutions. Nuclei were stained with Hoechst 33258 (Nacalai Tesque).

Histology

The fixed eyes, brains and kidneys (in 4% paraformaldehyde) were dehydrated, embedded in paraffin, and sectioned with a microtome. Hematoxylin and eosin (HE) staining or Nissl staining were carried out on paraffin sections using a standard procedure. Images were captured using the BX 51 microscopy system (Olympus, Tokyo, Japan) connected to a DP70 digital camera (Olympus).

Enzyme-linked immunosorbent assay

The concentrations of PDGF-AB, PDGF-BB, VEGF-A, and PlGF in the retinas of N-PRβ-KO or WT mice were measured by ELISA according to the manufacturer's instructions (R&D, Minneapolis, MN, USA). Briefly, collected retinas were snap-frozen in liquid nitrogen, smashed into a powder using the Multi-Beads Shocker (Yasui-kiki, Osaka, Japan), and lysed using T-PER Tissue Protein Extraction Reagent (Thermo Fisher Scientific Inc., Waltham, MA, USA) with Halt Protease Inhibitor Cocktail (Thermo Fisher Scientific Inc.). After centrifugation, lysates were used as samples. The concentrations of PDGF-AB, PDGF-BB, VEGF-A, and PlGF were calculated from the standard curve.

Image analysis and quantification

Images of HE sections of retinas were captured using an IX71 microscope (Olympus) and the retinal thickness of the peripheral area was measured using cellSens Standard (ver.1.4.1; Olympus). Images of the flat-mount immunostained retinas were captured using a LSM780 confocal system (Carl Zeiss) and a BZ-X700 microscope (Keyence). For immunofluorescence of CD31 and collagen type IV, the percentage of the whole retinal area (pixel) that was immunoreactive (pixel) was

analyzed using BZ-H3C software (Keyence). For pericyte coverage on the retinal vasculature, the percentage of area that was immunoreactive (pixel) for NG2, CD13, αSMA, and CD31 was analyzed using ImageJ (National Institutes of Health, Bethesda, MD, USA). For the analysis of western blotting data, the immunoreactive bands of target proteins were quantified using ImageJ (NIH) and normalized to the β-actin protein band.

Fig. S1

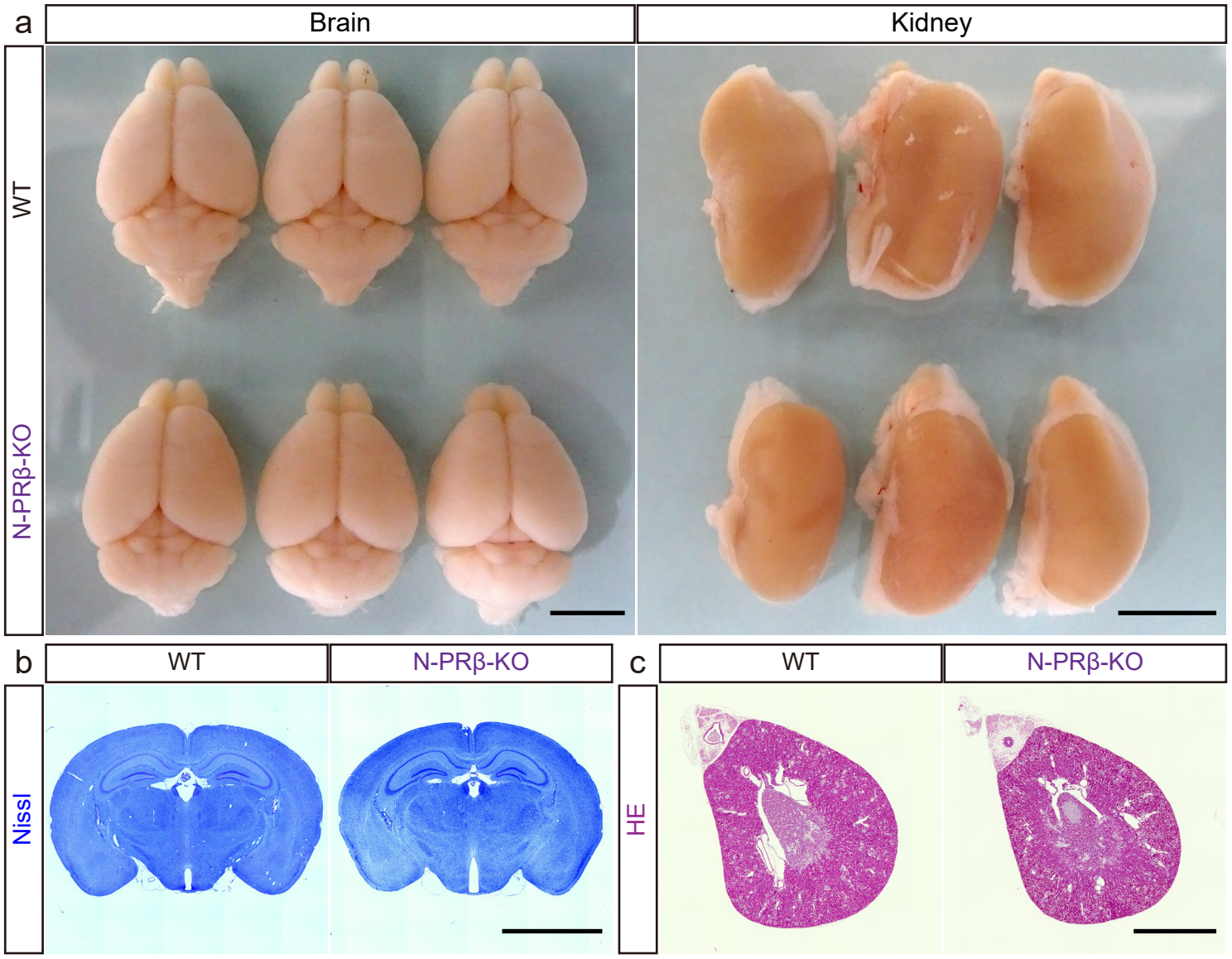

Fig. S1. Overview of the brain and kidney from N-PRβ-KO mice and histological analysis compared with WT mice. Related to Fig. 1

(a) Overview of the brain (left) and kidney (right) collected from WT and N-PRβ-KO mice at 8 weeks. While brains and kidneys of N-PRβ-KO (bottom row) were somewhat small sized compared with WT (upper row), no visible structural abnormality could be observed in N-PRβ-KO compared with WT. (b and c) In microscopic analysis using paraffin sections of brain (b, Nissl staining) and kidney (c, HE staining), no visible difference could be observed in N-PRβ-KO compared with WT. Scale bar = 5 mm (a and b), 2 mm (c).

Fig. S2

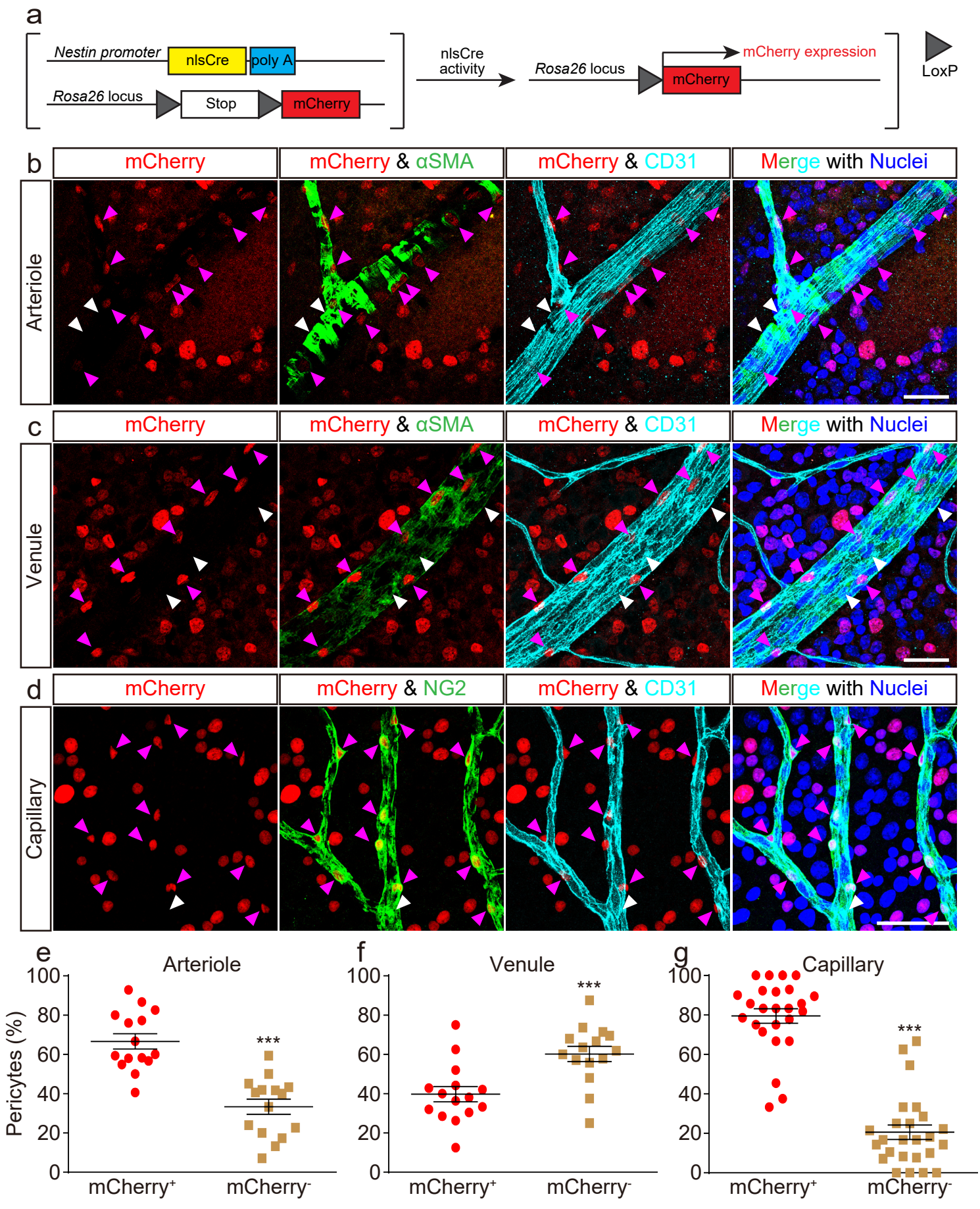
a
Nestin promoter
nlsCre
poly A
Rosa26 locus
Stop
mCherry
nlsCre activity
Rosa26 locus
mCherry expression
mCherry
LoxP
b
mCherry
mCherry & αSMA
mCherry & CD31
Merge with Nuclei
Arteriole
c
mCherry
mCherry & αSMA
mCherry & CD31
Merge with Nuclei
Venule
d
mCherry
mCherry & NG2
mCherry & CD31
Merge with Nuclei
Capillary
e
Arteriole
f
Venule
g
Capillary
Pericytes (%)
100
80
60
40
20
0
***
mCherry+
mCherry-

Fig. S2. N-MC retina shows both mCherry positive and negative retinal pericytes. Related to Fig. 2 and 5

(a) Schematic representation of the transgenic and mutated alleles of N-MC. mCherry expression controlled by a *Rosa26* promoter that is suppressed by two loxP sites flanking the stop codon is activated by nlsCre activity driven by the *Nestin* promoter. (b–d) mCherry (red) is expressed in pericytes enwrapping arteriole (b), venule (c) and capillary (d) (magenta-arrowheads), but $mCherry^{-}$ pericytes can be also observed among arteriole, venule and capillary (white-arrowheads) at 4 weeks. Pericytes are delineated by expression of αSMA (green, b and c) and NG2 (green, d). mCherry is also positive in the neuronal and glial cells. CD31-positive blood vessels (cyan), Hoechst-stained nuclei (blue). (e–g) Percentage of $mCherry^{+}$ and $mCherry^{-}$ pericytes on the retinal blood vessels of N-MC mice. $mCherry^{-}$ pericytes were significantly lower than $mCherry^{+}$ pericytes in arteriole and capillary (e and g). $mCherry^{-}$ pericytes were significantly higher than $mCherry^{+}$ pericytes in venule (f). n = 15 randomly selected areas of arterioles and venules, and 25 randomly selected areas of capillaries (40× objective lens) from 5 retinas of males and females. All values represent the mean ± SEM. ***, $p < 0.001$, compared to WT. Scale bar = 50 μm (b–d).

Fig. S3

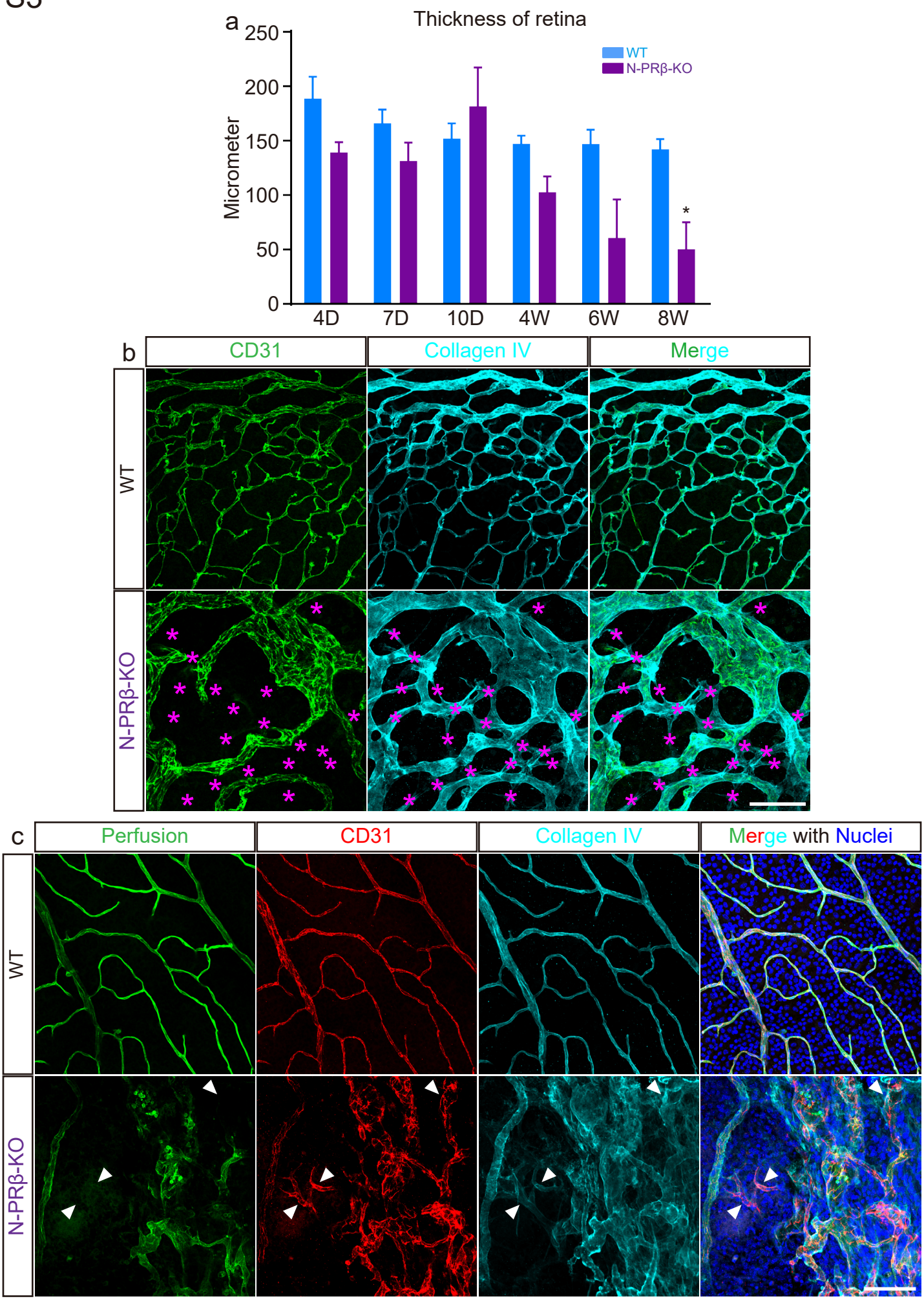
a
Thickness of retina
Micrometer
250
200
150
100
50
0
WT
N-PRβ-KO
*
4D
7D
10D
4W
6W
8W
b
CD31
Collagen IV
Merge
WT
N-PRβ-KO
c
Perfusion
CD31
Collagen IV
Merge with Nuclei
WT
N-PRβ-KO

Fig. S3. Retinal thinning and vascular abnormality in young aged N-PRβ-KO mice. Related to Fig. 3

(a) Peripheral region of the retinal thickness was comparable between WT and N-PRβ-KO mice from P4 to P10. However, N-PRβ-KO retinas gradually became thinner compared with WT mice from 4 weeks. n = 3–5 retinas collected from males and females at the indicated time points. (b) Whereas physiological blood vessel regression and some empty sleeves are observed in WT mice at 2 weeks, N-PRβ-KO mice show abnormally large blood vessel regression and drastic empty sleeve formation (indicated by asterisks in magenta) is found in many locations. CD31-positive blood vessels (green), collagen type IV-positive ECM (cyan). (c) Non-functioning retinal blood vessels in N-PRβ-KO mice. While all of retinal blood vessels are visualized by transcardially perfusion of IB4-Alexa488 (green) in WT at 4 weeks of age, non-functioning retinal blood vessels are observed in N-PRβ-KO (arrowheads). Retinal blood vessels are also visualized by CD31 (red) and collagen type IV (cyan) immunostainings. Nuclei are depicted by Hoechst (blue). All values represent means ± SEM. *, $p < 0.05$, compared to WT mice at the same time points. Scale bar = 100 μm (b and c).

Fig. S4

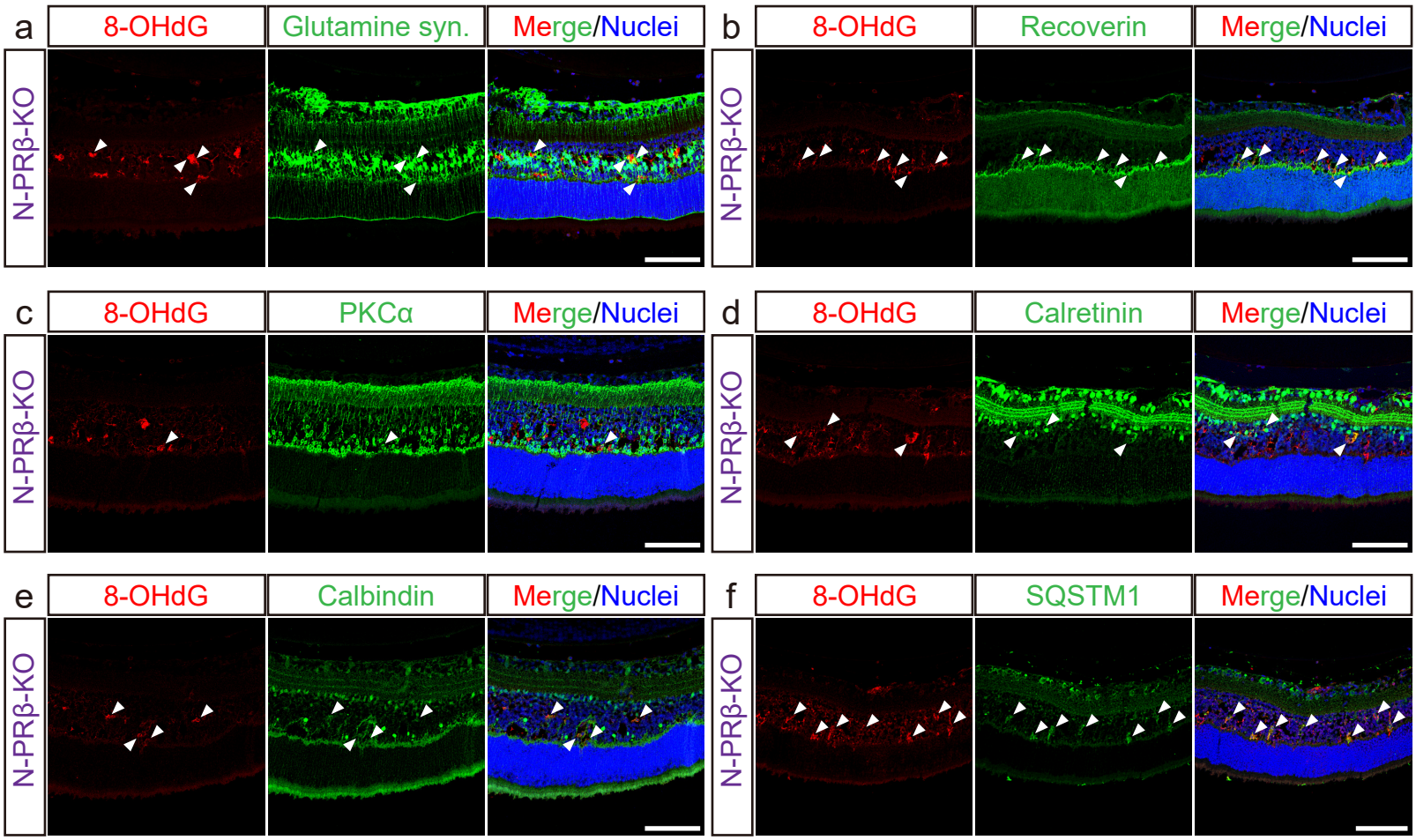
a
8-OHdG
Glutamine syn.
Merge/Nuclei
N-PRβ-KO
b
8-OHdG
Recoverin
Merge/Nuclei
N-PRβ-KO
c
8-OHdG
PKCα
Merge/Nuclei
N-PRβ-KO
d
8-OHdG
Calretinin
Merge/Nuclei
N-PRβ-KO
e
8-OHdG
Calbindin
Merge/Nuclei
N-PRβ-KO
f
8-OHdG
SQSTM1
Merge/Nuclei
N-PRβ-KO

Fig. S4. Retinal structural defects of N-PRβ-KO mice caused by oxidative stress. Related to Fig. 3

(a–e) Immunolabeling of 8-OHdG (red) depicts oxidative stress in the inner nuclear layer of N-PRβ-KO retinas at 2 weeks. Müller cells (a), photoreceptors (b), bipolar cells (c), amacrine cells (d), and horizontal cells (e) are immunolabeled using specific antibodies (green), and co-express 8-OHdG (arrowheads). Hoechst delineates nuclei (blue). (f) 8-OHdG-positive cells (red) co-express SQSTM1 (green, arrowheads), an autophagy marker. Hoechst delineates nuclei (blue). Scale bar = 100 μm (a–f).

Fig. S5

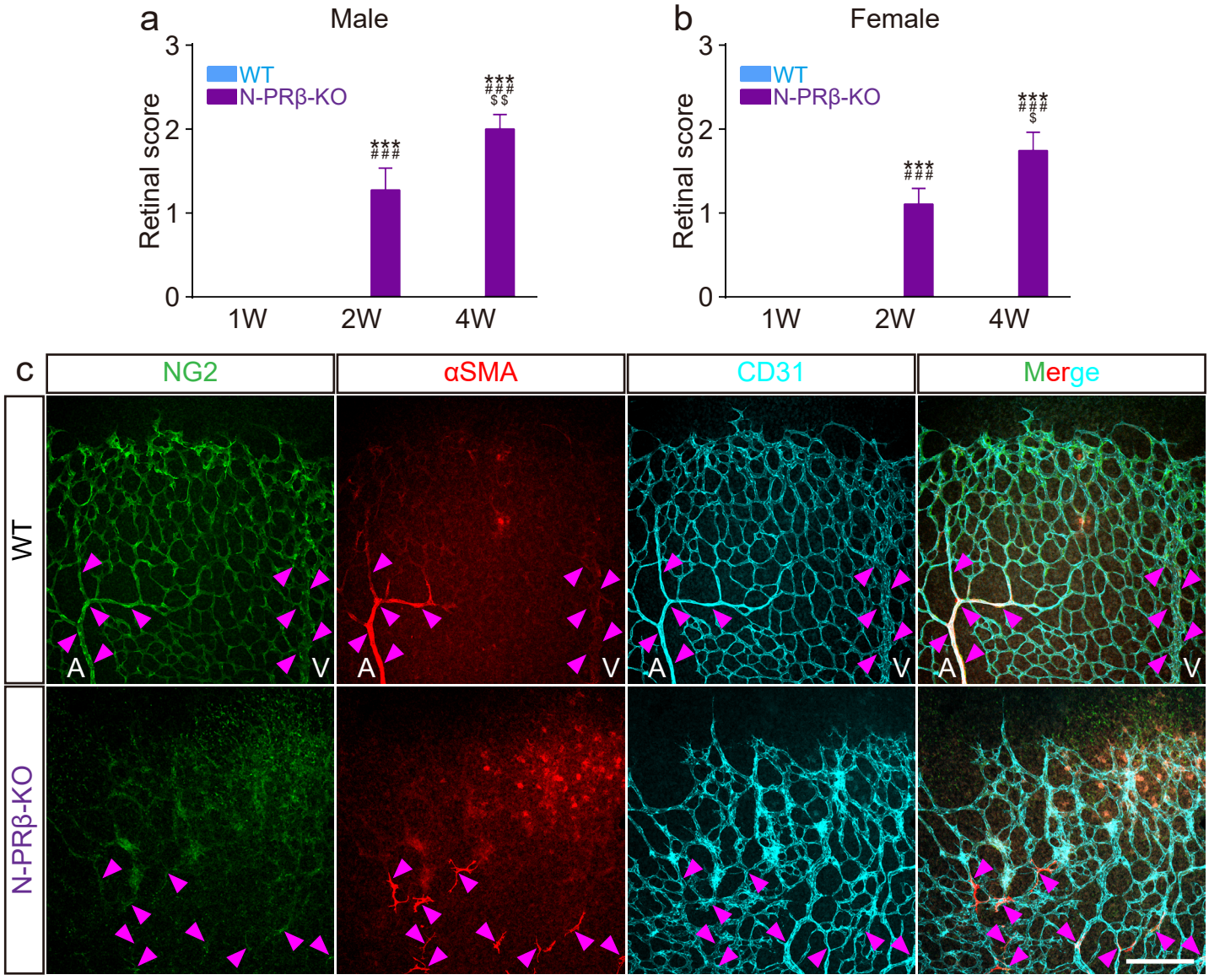

d

Retinal hemorrhage in N-PRβ-KO

Age	Number	Score				
		O	I	II	III	IV
1 week	55	87.3% (48/55)	0% (0/55)	9.1% (5/55)	3.6% (2/55)	0% (0/55)
2 weeks	56	25.0% (14/56)	0% (0/56)	14.3% (8/56)	5.4% (3/56)	55.4% (31/56)
4 weeks	102	16.7% (17/102)	0% (0/102)	21.6% (22/102)	7.8% (8/102)	53.9% (55/102)
6-12 weeks	75	28.0% (21/75)	0% (0/75)	10.7% (8/75)	22.7% (17/75)	38.7% (29/75)
4 months - 1 year	77	39.0% (30/77)	24.7% (19/77)	18.2% (14/77)	3.9% (3/77)	14.3% (11/77)

Fig. S5. Scoring of retinal defects in young age and hemorrhage in N-PRβ-KO mice. Related to Fig. 3

(a and b) Retinal defects of N-PRβ-KO male (a) and female mice (b) at 1 to 4 weeks were evaluated based on retinal evaluation scores as described in Figure 1d. All values represent means ± SEM. ***, $p < 0.001$ vs. WT mice at the same time points, $^{###}$, $p < 0.001$ vs. N-PRβ-KO mice at 1 week, $^{\$}$, $p < 0.05$; $^{\$\$}$, $p < 0.01$ vs. N-PRβ-KO mice at 2 weeks. (c) Multi-color immunofluorescence of vascular front at 1 week. In WT mice (upper row), many $NG2^+\alpha SMA^-$ pericytes were recruited in microcapillaries of retinal vascular front. $NG2^+\alpha SMA^+$ pericytes (arrowheads) preferentially enwrapped arterioles (A) and venules (V). In contrast, in N-PRβ-KO vascular front, almost all $NG2^+\alpha SMA^-$ pericytes disappeared from microcapillaries. In the same mice, fewer $NG2^+\alpha SMA^+$ pericytes (arrowheads) were aberrantly distributed that did not form normal arteriolar or venular structures (arrowheads). Scale bar = 200 μm. (d) N-PRβ-KO mice frequently show retinal hemorrhage. After perfusion fixation under deep anesthesia, the lenses were removed from the excised eyeballs, and hemorrhage phenotypes were examined with a stereomicroscope (Olympus SZ61, Osaka, Japan). After examining extensive samples, hemorrhages were classified as per the following criteria, and occurrence was evaluated.

O: Signs of hemorrhage are not detected.

I: Traces of pre-existing hemorrhage are detected based on yellowish-brown deposition on the retinal surface.

II: Fresh hemorrhage, a thin layer of red fluid spreads on the retinal surface.

III: Fresh hemorrhage, a thick layer of red fluid is clearly visible on the retinal surface.

IV: Large hemorrhage with pooled blood within the eyeball.

Fig. S6

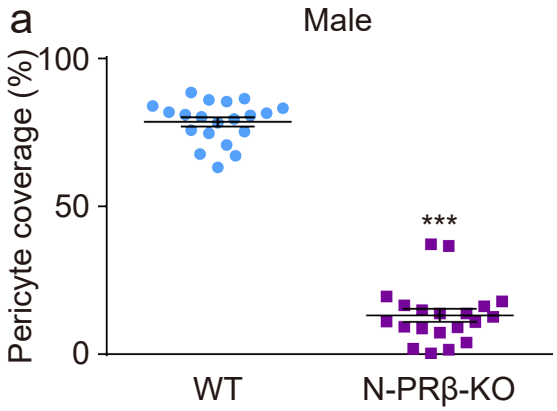
a
Male
Pericyte coverage (%)
100
50
0
***
WT
N-PRβ-KO

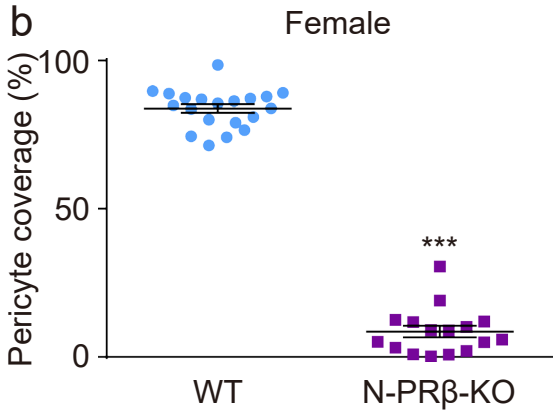
b
Female
Pericyte coverage (%)
100
50
0
***
WT
N-PRβ-KO

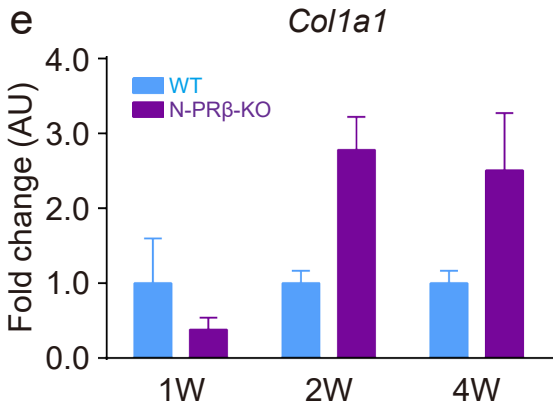
e
Col1a1
Fold change (AU)
4.0
3.0
2.0
1.0
0.0
WT
N-PRβ-KO
1W
2W
4W

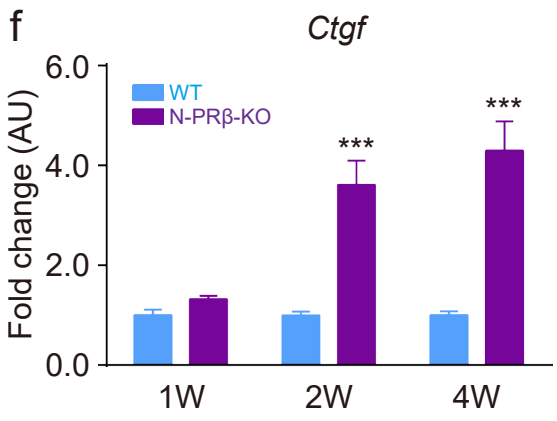
f
Ctgf
Fold change (AU)
6.0
4.0
2.0
0.0
WT
N-PRβ-KO
***
***
1W
2W
4W

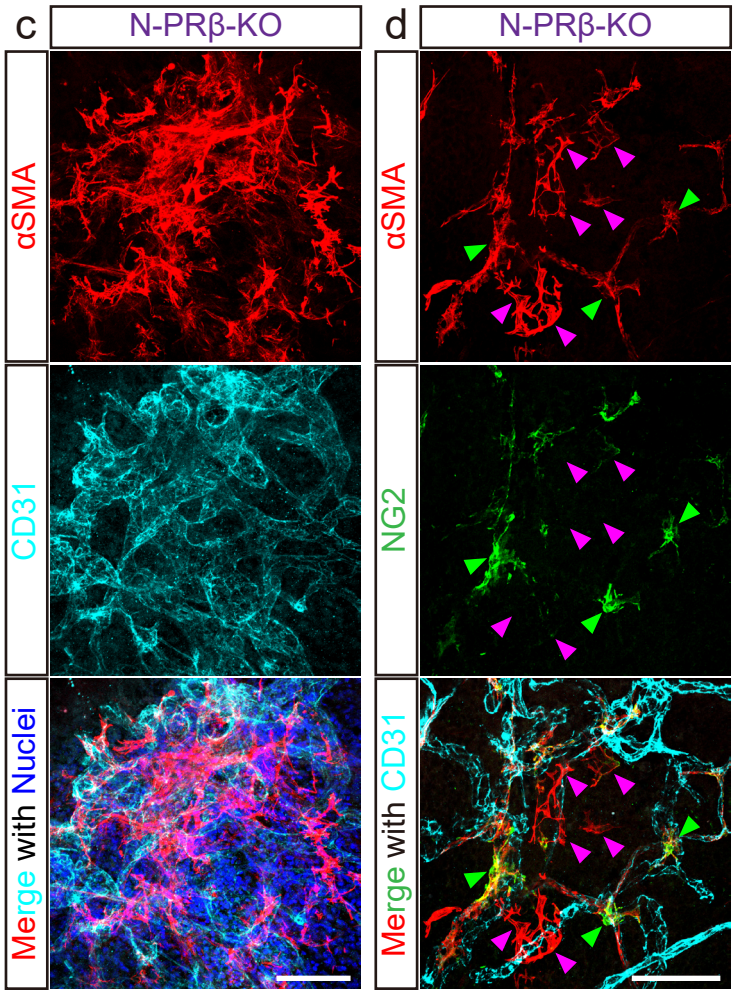
c
N-PRβ-KO
d
N-PRβ-KO
αSMA
CD31
NG2
Merge with Nuclei
Merge with CD31

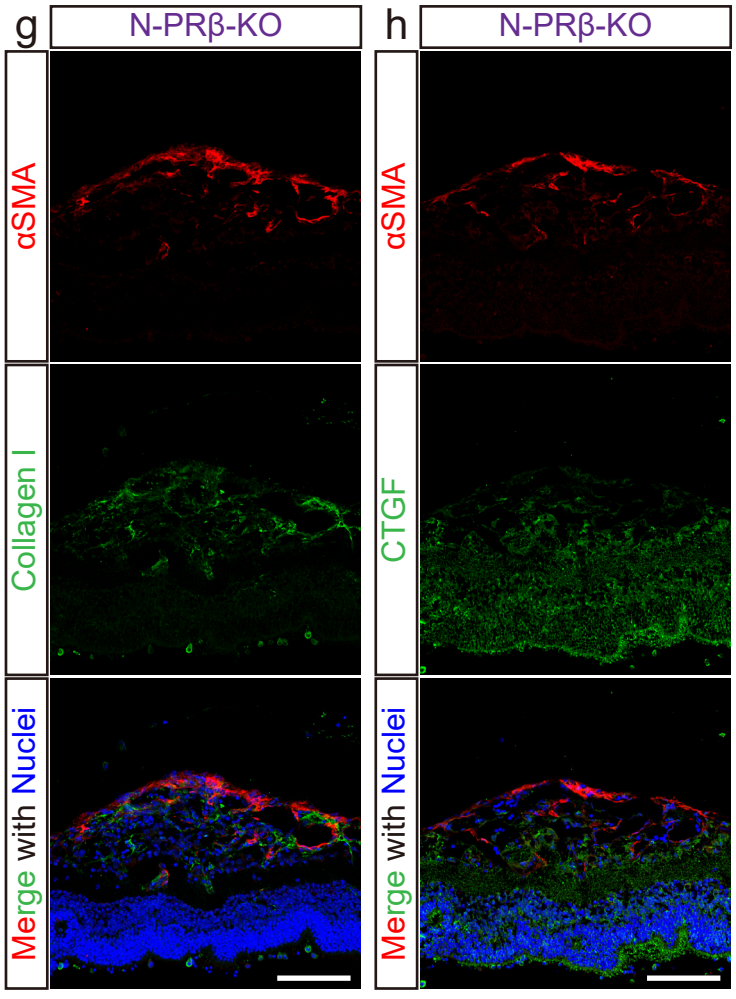
g
N-PRβ-KO
h
N-PRβ-KO
αSMA
Collagen I
CTGF
Merge with Nuclei

Fig. S6. Pericyte coverage and proliferative membrane formation in young aged N-PRβ-KO mice. Related to Fig. 3 and 5

(a and b) Percentage of $NG2^+$ pericyte coverage on the retinal vasculature of N-PRβ-KO mice. Pericyte coverage was significantly lower in N-PRβ-KO mice than WT mice for both males (a) and females (b) at 4 weeks. n = 16–20 randomly selected areas (20× objective lens) from 4–5 retinas of males and females. (c and d) In N-PRβ-KO mice but not WT mice, αSMA^+ pericytes (red, myofibroblast-like phenotype) constitute foci of the proliferative membrane at 4 weeks (c). CD31-positive blood vessels (cyan), Hoechst-stained nuclei (blue). $NG2^+\alpha SMA^+$ pericytes detach from retinal blood vessels (cyan), and decrease NG2 (green) and appear to increase αSMA (red) expression at 4 weeks (d). Green-arrowheads show $NG2^+\alpha SMA^+$ pericytes that adhere to the blood vessels. Magenta-arrowheads indicate $NG2^{dim/-}\alpha SMA^+$ pericytes that are detaching from blood vessels. The sequential phenotypic change indicates PFT. (e and f) Real-time PCR analyses of *Col1a1* mRNA (e) and *Ctgf* mRNA (f) that are upregulated in fibrotic tissues. Both of them highly induced in N-PRβ-KO mice at 2 and 4 weeks compared with those of WT mice. (g and h) Immunofluorescence of collagen type I (g) and CTGF (h) using sections of N-PRβ-KO retinas at 4 weeks. Collagen type I exclusively expressed in foci of proliferative membrane. CTGF were diffusely expressed in foci of proliferative membrane and degenerated retina. All values represent means ± SEM. ***, $p < 0.001$ vs. WT mice at the same time points. Scale bar = 100 μm (c, d, g and h).

Fig. S7

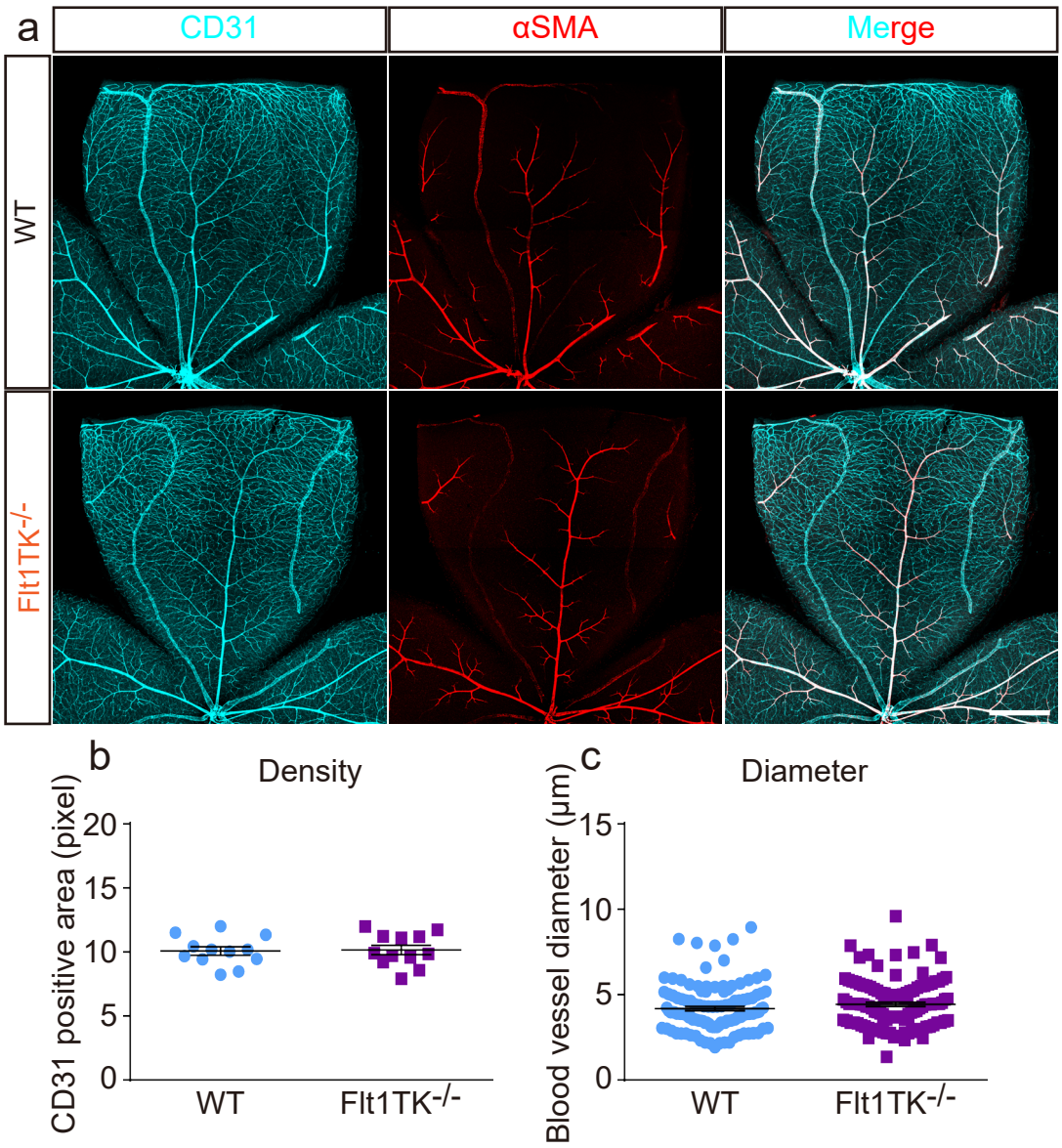
a
CD31
αSMA
Merge
WT
Flt1TK-/-
b
Density
CD31 positive area (pixel)
20
15
10
5
0
WT
Flt1TK-/-
c
Diameter
Blood vessel diameter (μm)
15
10
5
0
WT
Flt1TK-/-

Fig. S7. *Flt1TK*$^{-/-}$ mice show intact retinal vasculature in physiological condition. Related to Fig. 7

(a) Distribution of CD31^{+} retinal blood vessels (cyan) and localization of αSMA^{+} pericytes (red) are similar levels in both WT and *Flt1TK*$^{-/-}$ mice at 4 weeks. Scale bar = 500 μm. (b and c) The *Flt1TK*$^{-/-}$ retinal blood vessel area was comparable compared to the WT (b). n = 12 randomly selected areas (20× objective lens) from 4 retinas collected from males and females. The blood vessel diameter of *Flt1TK*$^{-/-}$ retinas was similar to WT (c). n = 120 randomly selected blood vessels (20× objective lens) from 4 retinas collected from males and females. All values represent means ± SEM.